Swansea University
Prifysgol Abertawe

Cronfa
Setting Research Free

Cronfa - Swansea University Open Access Repository

This is an author produced version of a paper published in:
The Journal of Physical Chemistry C

Cronfa URL for this paper:
http://cronfa.swan.ac.uk/Record/cronfa50063

Paper:
Pockett, A., Raptis, D., Meroni, S., Baker, J., Watson, T. & Carnie, M. (2019). Origin of Exceptionally Slow Light Soaking Effect in Mesoporous Carbon Perovskite Solar Cells with AVA Additive. *The Journal of Physical Chemistry C, 123*(18), 11414-11421.
http://dx.doi.org/10.1021/acs.jpcc.9b01058

Released under the terms of a Creative Commons Attribution License (CC-BY).

This item is brought to you by Swansea University. Any person downloading material is agreeing to abide by the terms of the repository licence. Copies of full text items may be used or reproduced in any format or medium, without prior permission for personal research or study, educational or non-commercial purposes only. The copyright for any work remains with the original author unless otherwise specified. The full-text must not be sold in any format or medium without the formal permission of the copyright holder.

Permission for multiple reproductions should be obtained from the original author.

Authors are personally responsible for adhering to copyright and publisher restrictions when uploading content to the repository.

http://www.swansea.ac.uk/library/researchsupport/ris-support/

This is an open access article published under a Creative Commons Attribution (CC-BY) License, which permits unrestricted use, distribution and reproduction in any medium, provided the author and source are cited.

THE JOURNAL OF PHYSICAL CHEMISTRY C

Article

Cite This: J. Phys. Chem. C 2019, 123, 11414−11421

pubs.acs.org/JPCC

Origin of Exceptionally Slow Light Soaking Effect in Mesoporous Carbon Perovskite Solar Cells with AVA Additive

Adam Pockett,* Dimitrios Raptis, Simone M. P. Meroni, Jenny Baker, Trystan Watson, and Matthew Carnie*

Materials Research Centre, College of Engineering, SPECIFIC−Swansea University, Bay Campus, Swansea, SA1 8EN, United Kingdom

Supporting Information

ABSTRACT: A range of slow dynamic processes occurring in perovskite solar cells have been linked to ionic migration, including $J-V$ hysteresis and long photovoltage rise and decay times. This work demonstrates the remarkably slow response time of triple mesoporous carbon-based cells, containing the additive 5-aminovaleric acid iodide (AVA). The photovoltage rise under illumination is 1−2 orders of magnitude longer than has previously been observed for planar and mesoporous TiO_2 based devices. Transient photovoltage measurements during this slow rise in voltage show a strong negative transient feature which demonstrates the presence of fast recombination. By analyzing the rate of V_{oc} rise and the decay of this negative transient, we show a clear link between this recombination process and the limiting of the V_{oc}. The reduction of recombination over time and the resultant rise in V_{oc} are influenced by the movement of ions in the perovskite. From temperature-dependent measurements, an activation energy consistent with previous literature values for iodide ion migration is obtained, although the attempt frequency is found to be many orders of magnitude lower than that in pure MAPI perovskite devices. We attribute this to the presence of the AVA molecule inhibiting the movement of ions. The importance of the TiO_2/ZrO_2 interface in leading to this slow behavior is revealed by studying devices with different architectures with and without the AVA additive. A significant increase in response time can only be recreated in a device with both of the mesoporous metal oxide layers and the AVA additive present in the perovskite.

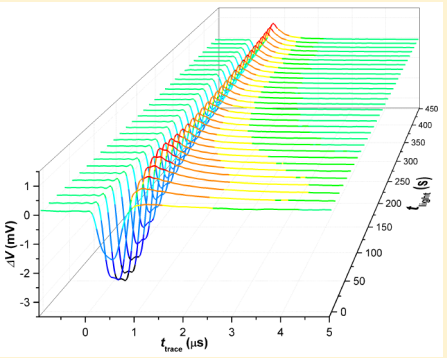

INTRODUCTION

Since the introduction of solid-state perovskite photovoltaic devices in 2012, there has been rapid progress in the record efficiencies of lab-scale devices. In general, many of the devices at or near these record efficiencies in excess of 20% share a similar device architecture. They predominantly consist of a series of spin-coated layers, often including expensive organic transport layers with evaporated metal contacts. Major challenges for the scale-up of perovskite devices therefore include the following: the reduction of material costs, the use of larger scale deposition methods, and a lower capital expenditure requirement compared to a vacuum process such as thermal evaporation. There are numerous scale-up activities taking place using a range of approaches including slot-die coating,[1−3] inkjet printing,[4,5] evaporation,[6,7] and screen printing.[8−10] Perhaps the most promising architecture for addressing the main challenges to large scale production are the carbon-based hole transport layer free devices introduced by Ku et al.[9] These devices consist of three screen printed mesoporous layers (TiO_2, ZrO_2, and carbon) which are then infiltrated with a perovskite solution.[11] Large area modules have already been demonstrated using this architecture,[12] although record device efficiencies still linger some way behind those of spin-coated cells with evaporated metallic contacts.[13]

Device stability is another challenging factor facing the commercialization of perovskite solar cells. The "original" lead halide perovskite, methylammonium lead iodide (MAPI), has been shown to be thermodynamically unstable,[14] as well as also being susceptible to degradation induced by exposure to light, oxygen, and moisture.[15,16] Stability can be improved by substitution of some of the methylammonium with other cations such as cesium and formamidinium.[17] The addition of larger cations, such as butylammonium or 2-phenylethylammonium, disrupts the standard 3D perovskite and leads to the formation of a 2D structure. Depending on the relative concentration of these cations, layers of 2D/3D perovskite regions can be formed.[18,19] Long chain cations can form hydrophobic interlayers between regions of 3D perovskite, offering greater stability to moisture.[20]

The benefits of a 2D/3D perovskite material in a triple mesoporous carbon-based device has been highlighted by Grancini et al.[21] The addition of a relatively low concentration (3% AVA:PbI_2) of 5-aminovaleric acid iodide (AVA), in the MAPI solution infiltrated into the mesoporous scaffold,

Received: February 1, 2019
Revised: April 16, 2019
Published: April 18, 2019

Downloaded via SWANSEA UNIV on May 9, 2019 at 15:14:40 (UTC).
See https://pubs.acs.org/sharingguidelines for options on how to legitimately share published articles.

© 2019 American Chemical Society

DOI: 10.1021/acs.jpcc.9b01058
J. Phys. Chem. C 2019, 123, 11414−11421

improved performance and stability. Indeed, this device set the record for long-term stability, showing no appreciable degradation after 10 000 h under full simulated sunlight at elevated temperatures. While the presence of the AVA in the perovskite solution clearly had an impact on the final material, it was not possible to observe the formation of a 2D phase from X-ray diffraction measurements for such a low concentration of the cation—it was believed that the 2D layer would have been too thin to resolve. Due to the presence of a carboxylic acid group on the AVA molecule, it was assumed that it would be likely to adsorb to the metal oxide interface and template the growth of the 2D/3D perovskite.

It has become apparent that triple mesoporous carbon based cells containing the AVA additive can require extensive periods of preconditioning in order to measure the optimum *JV* parameters.[22,23] It is typical to light soak the devices for several minutes before measuring. Such slow dynamic behavior immediately suggests a link to the effects of ion migration, as has been observed in numerous measurements, most commonly manifesting as hysteresis in the *JV* curve.[24−28]

We have previously demonstrated the role of surface recombination, at the perovskite/TiO_2 interface, and ionic migration in contributing to hysteresis and other slow electrical responses such as a slow rise in open-circuit voltage under illumination.[29] It was shown that a negative deflection (short-lived decrease in V_{oc}) in the transient photovoltage measurements in response to the laser pulse was due to an increase in the recombination rate caused by an increase in the accumulation of holes at the TiO_2 interface. This effect was dominant immediately after turning on the background illumination following the cell being at equilibrium in the dark. The amplitude of the negative deflection decreased slowly over time, with a rate strongly dependent on temperature and consistent with the slow rise in V_{oc}. This suggested the suppression of the open-circuit voltage due to surface recombination, which reduced over time on time scales consistent with ionic motion.

In this work, we will show that a similar process is present in the triple mesoporous carbon-based devices, and we will show how the device structure and most notably the presence of the AVA additive exacerbates the impact. We observe a strong negative photovoltage transient response during the slow rise of V_{oc} under illumination. The time constant of this process is 1−2 orders of magnitude longer than previously observed in planar perovskite devices. However, calculation of the activation energy for this process reveals that it has similar origins; i.e., it is linked to migration of iodide ion vacancies. It appears that the presence of the AVA molecule inhibits ion migration by reducing the attempt frequency. In order to study the origins of this extremely slow behavior, we fabricate devices using spiro-OMeTAD as the hole transport layer (HTL) and different combinations of mesoporous TiO_2 and/or ZrO_2. It is revealed that the order of magnitude increase in time constant can only be recreated in devices containing TiO_2 and ZrO_2 mesoporous layers with the AVA additive present in the perovskite. This suggests that the AVA may be preferentially adsorbed at the TiO_2/ZrO_2 interface.

EXPERIMENTAL SECTION

Meso-C Device Preparation. Laser patterned substrates were cleaned using Hellmanex detergent (5% in deionized water), rinsed with deionized water, acetone and 2-propanol and dried with nitrogen, then plasma cleaned for 10 min using a Nano plasma system (Diener Electronics). A compact TiO_2 BL was deposited by spraying a 0.2 M titanium diisopropoxide bis(acetylacetonate) solution in 2-propanol onto the FTO substrates kept at 300 °C on a hot plate. A commercial TiO_2 paste (Dyesol 30-NRD diluted 1:1 in terpineol) was screen printed and then sintered at 550 °C for 30 min, to obtain an 800 nm mesoporous TiO_2 layer. A 1.2 μm zirconia layer was deposited afterward by screen printing (Solaronix ZT/SP) and heated at 400 °C for 30 min, followed by the screen printing of the carbon paste (GEM D3) to get a 10 μm top electrode, which was then also annealed at 400 °C for 30 min. The substrates were cooled down and kept at 150 °C until ready for the infiltration of the perovskite solution. All layers were printed in air under ambient conditions.

An equimolar solution of PbI_2 (TCI Chemicals) and MAI (Dyesol) in γ-butyrolactone (Sigma-Aldrich) was prepared by adding 5-AVAI (Dyesol) to obtain a 3% molar ratio between 5-AVAI and MAI and was drop casted on the cells through the carbon layer. After 30 min to allow the solution to percolate throughout the triple stack, the devices were annealed in a fan oven for 1 h and 45 min at 50 °C.

Standard Device Preparation. Substrate cleaning and compact TiO_2 BL deposition was carried out as above. Mesoporous TiO_2 and ZrO_2 layers were spin coated using the same Dyesol and Solaronix pastes but diluted with ethanol in a 1:2.5 ratio to obtain layer thicknesses of 400 nm for each. Annealing of these layers was also carried out as above. The perovskite layer was deposited by spin coating a 1.25 M solution of MAI and PbI_2 in a 4:1 (v:v) mixture of DMF and DMSO, at 4000 rpm for 30 s. The 5-AVAI was used in the same 3% molar ratio to MAI. Ethyl acetate was used as the antisolvent during spin coating. Spiro-OMeTAD (90 mg/mL) in chlorobenzene (additives: 30 μL ml^{-1} tBP, 20 μL ml^{-1} Li-TFSI solution [0.6 M Li-TFSI in acetonitrile], 20 μL ml^{-1} FK209 solution [0.6 M FK209 in acetonitrile]) was spin coated at 4000 rpm for 30 s. Gold electrodes were deposited by thermal evaporation.

IV Characterization. Masked devices (0.5 cm^2 for meso-C, 0.1 cm^2 standard cells) were tested under a class AAA solar simulator (Newport Oriel Sol3A) at AM1.5 100 mW cm^{-2} illumination conditions (calibrated using a KG5 filtered reference cell) using a Keithley 2400 source meter. The devices were scanned from V_{oc} to J_{sc} and vice versa at a scan rate of 330 mV s^{-1}, after 3 min of light soaking.

TPV Characterization. TPV measurements were performed using a commercially available transient measurement system (Automatic Research GmbH). This system uses a 635 nm red laser diode driven by a waveform generator (Keysight 33500B). The laser pulse length was adjusted (typically 500 ns) to study different features of the transient response. Background illumination was provided by a white LED with its intensity calibrated to generate the same device photocurrent as measured using the solar simulator—this intensity is referred to as 1 sun equivalent.

Measurements were initiated once devices had equilibrated in the dark for up to tens of minutes (until V_{oc} measured less than 1 mV). The white bias light and laser diode were turned on using a fast MOSFET and optical shutter, respectively, both of which were controlled by the same trigger source. TPV traces were recorded at regular intervals (typically 0.5−1 s) by a Tektronix DPO3012 oscilloscope controlled by Tektronix SignalExpress software. The device under test is held at open-

DOI: 10.1021/acs.jpcc.9b01058
J. Phys. Chem. C 2019, 123, 11414−11421

circuit by a custom-built voltage follower (1.5 TΩ input impedance).

Temperature controlled transient measurements were performed using an Oxford Instruments Optistat DN2 cryostat cooled with liquid nitrogen, with the sample under vacuum.

RESULTS AND DISCUSSION

The initial transient photovoltage response upon illumination with the white bias LED for a meso-C device containing the AVA additive is shown in Figure 1. This trace is captured after

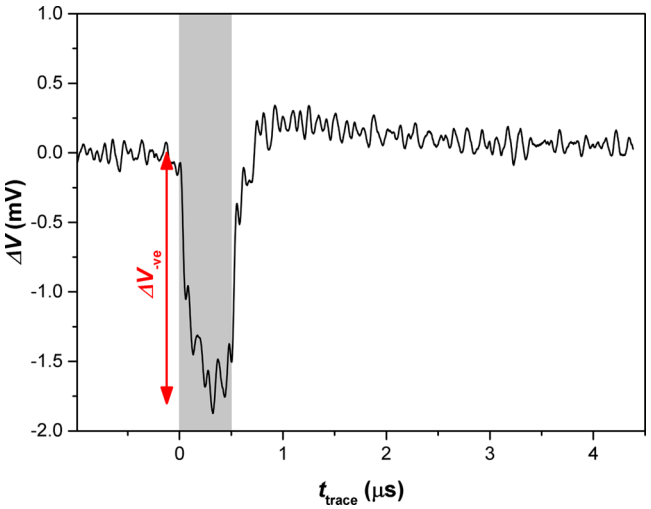

Figure 1. Initial TPV response after bias illumination is turned on for a meso-C cell with AVA additive. Shaded region indicates timing of laser pulse. ΔV_{-ve} represents the amplitude of the negative transient feature.

the near-instantaneous rise of the V_{oc} upon illumination (V_{oc} = 0.67 V), to a value lower than the final steady state V_{oc} ($V_{oc,steady\ state}$ = 0.75 V). The laser pulse induces a significant negative deflection in the TPV trace indicating a fast transient reduction in the open-circuit voltage caused by increased recombination. Once the laser pulse is extinguished, the V_{oc} recovers to a positive ΔV before decaying to a steady state. As shown previously, the excess charge carriers generated by the laser pulse can lead to increased surface recombination if the ionic distribution causes the electric field in the device to drive carriers toward the wrong contact, i.e., holes accumulate at the electron extracting contact.[29] The ions redistribute as a result of the Fermi-level splitting due to the bias illumination. This typically leads to the accumulation and subsequent recombination rate of these charges decreasing. The negative transient feature therefore diminishes on time scales related to the movement of ions.

The progression of the transient photovoltage response over time under bias illumination is shown in Figure 2. The magnitude of the negative response initially increases to a maximum value before decreasing slowly toward zero. This suggests that the variation in recombination rate involves a complex process in these devices and does not simply decrease over time as alluded to in previous works on planar devices.[29,30] The time scale for this behavior is also much longer than previously observed. When this process was previously studied in planar devices, it was necessary to cool the devices to 223 K in order to slow the voltage rise to allow measurements of the negative transient response for up to a

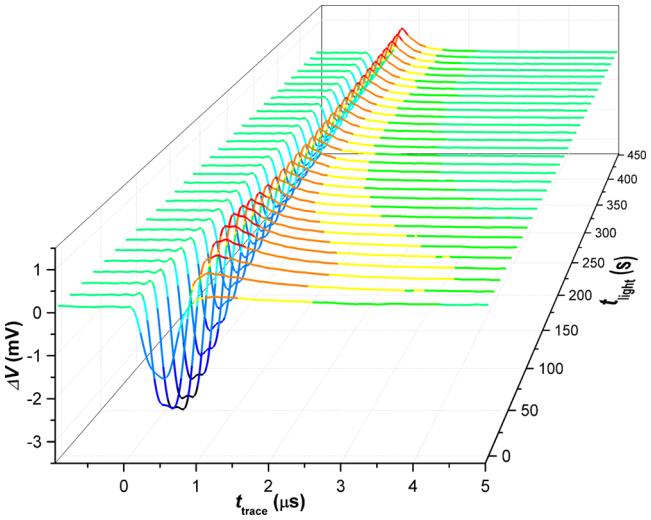

Figure 2. Progression of TPV transients during slow V_{oc} rise in a meso-C cell containing AVA additive under 1 sun equivalent light intensity at T = 303 K (t_{trace} is the time-base for each transient; t_{light} is the time since white bias light was switched on).

few hundreds of seconds. In the case of the AVA meso-C devices studied here, it was necessary to heat them to temperatures above room temperature to allow significant changes to be observed. Figure 2 shows that, even at 303 K, the TPV response is still varying on time scales on the order of minutes.

A clear link between the negative transient feature and the suppression of V_{oc} can be seen in Figure 3. There is a good

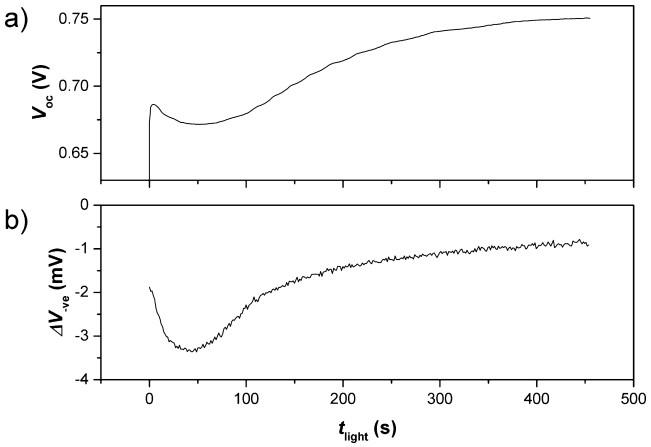

Figure 3. Slow part of the V_{oc} rise under illumination for a meso-C cell under 1 sun equivalent light intensity (a) and the corresponding amplitude of the negative "spike" in the transient measurement (as illustrated in Figure 1) (b).

qualitative agreement between the V_{oc} (Figure 3a) and the magnitude of the negative transient spike (Figure 3b). This shows that when the recombination rate is highest (maximum in negative transient amplitude observed at 45 s after illumination) the suppression of the V_{oc} is greatest (minimum of dip in V_{oc}). The whole profile of the V_{oc} rise and the amplitude of the negative transient over time are very similar. Again, this also highlights the slow rate of the process governing this behavior: at 303 K, the V_{oc} has not reached a

DOI: 10.1021/acs.jpcc.9b01058
J. Phys. Chem. C 2019, 123, 11414−11421

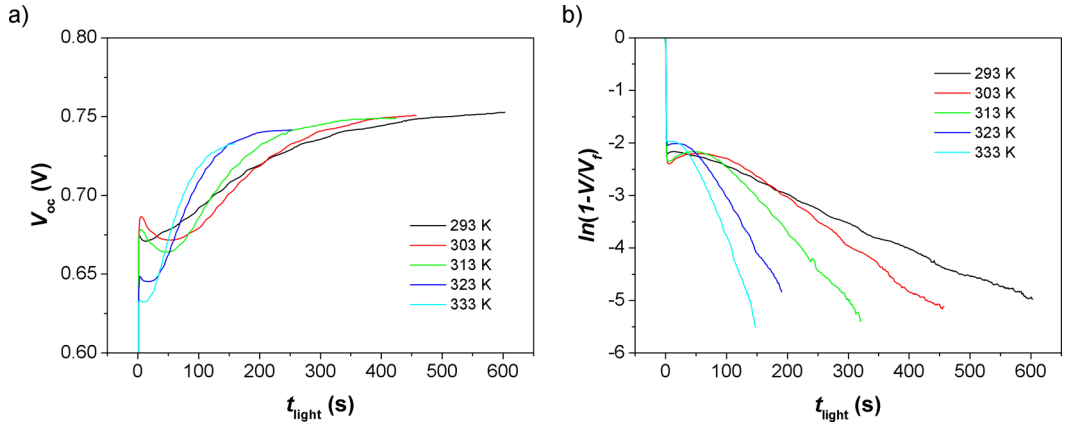

Figure 4. V_{oc} rise at different temperatures (a). V_{oc} rise plotted as function $\ln(1 - V/V_f)$ to highlight change of rate at different temperatures (b).

steady state nor has the negative feature diminished completely after 450 s of illumination.

The relationship between mobile ions and the observation of a range of slow dynamic behaviors have been previously studied by investigating the temperature dependence of the processes in question. This has included chronoamperometry,[24] thermally stimulated current,[31] impedance spectroscopy,[25] conductivity,[32] and open-circuit photovoltage rise and decay measurements.[25]

A strong temperature dependence of the V_{oc} rise under illumination can be seen for the AVA meso-C cells in Figure 4a. The V_{oc} rise at room temperature (293 K) has not reached a steady state after 10 min of illumination. At higher temperatures, the rise is significantly faster; at 323 K, the V_{oc} has reached a plateau after 200 s. The dip during the V_{oc} rise also changes in magnitude and timing for different temperatures; the analysis of this is beyond the scope of this work and would likely only be possible with sophisticated drift-diffusion modeling.

During the majority of the V_{oc} rise (after initial spike and dip) the increase in voltage is approximately monoexponential as can be seen in Figure 4b when the rise is plotted as a function, $\ln(1 - V/V_f)$, to analyze the rate at which the voltage, V, approaches a maximum steady state value, V_f. The rate is extracted by making a fit to the linear section of each curve. While there is a significant deviation from this linearity at shorter times, the linear region (single exponential behavior) extends for at least 100 s for the faster rise at 333 K and up to 400 s at 293 K.

The rate values for the voltage rise at each temperature are plotted in an Arrhenius plot in Figure 5. This shows clear Arrhenius behavior, with an activation energy of 0.37 eV. A wide range of activation energies for iodide ion migration via vacancies exist in literature. Values derived from first-principles range from 0.08 to 0.58 eV.[24,26,33,34] Experimental values range from 0.10 to 0.72 eV.[24,25,35,36] Such a widespread in values is perhaps expected due to the variety of computational and experimental techniques used. Experimental values are dependent on the exact material properties effecting the defect formation energy as well as the actual energy barrier to migration.[37,38] Computational values may also vary due to different assumptions and calculation of the formation energy of defects. Nevertheless, the value obtained in this study is within the range of literature values for the migration of iodide ions in perovskite.

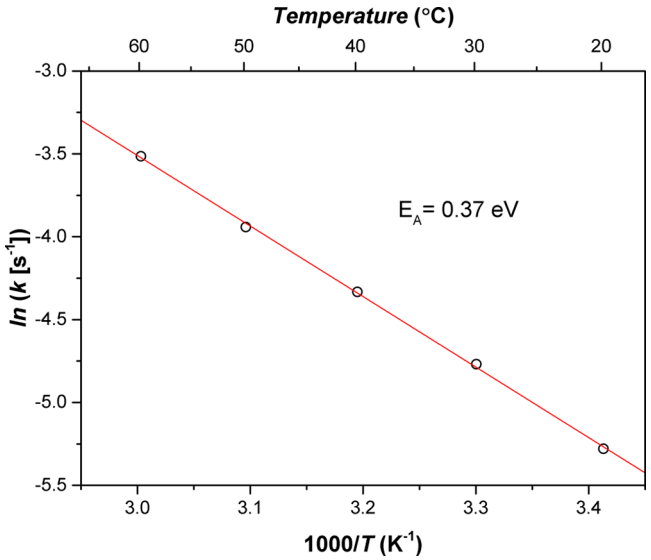

Figure 5. Arrhenius plot of rate of V_{oc} rise at different temperatures.

Calculation of the attempt frequency for ion migration, from the pre-exponential factor in the Arrhenius equation, gives a value of 1.1×10^4 s^{-1}. This is many orders of magnitude lower than values calculated from first-principles for pure MAPI perovskite, which are typically around 10^{12} s^{-1}.[24,26] It is possible that the presence of the AVA additive in the perovskite is hindering ion migration resulting in the much lower attempt frequency. This would also be consistent with the improved device stability with the use of the AVA, as degradation pathways such as superoxide formation are mediated by iodide vacancies.[39]

We have shown that the extremely slow electrical response of the AVA meso-C cells is linked to the migration of ions (presumably iodide vacancies) at much slower rates than observed for pure MAPI perovskite devices. In order to locate the dominant recombination process associated with this ion movement, we studied the impact of the AVA additive in cells with a more standard architecture. Specifically, this involved replacing the carbon electrode with spiro-OMeTAD and a gold evaporated contact. In our previous work, this contact was shown not to contribute to the negative transient behavior and eliminates the carbon electrode as a potential factor in this behavior in these devices.[29] The metal oxide layers were spin coated to allow faster optimization of the layer thicknesses; the

DOI: 10.1021/acs.jpcc.9b01058
J. Phys. Chem. C 2019, 123, 11414−11421

resultant layer thicknesses were around 400 nm each for mesoporous TiO_2 and ZrO_2—around half the thickness of these layers in the screen-printed cells. It was not possible to produce working devices with substantially thicker layers due to limitations of the spin coating method. We consider these thicknesses to be representative of the carbon-based devices, and more importantly the ratio between the two mesoporous layer thicknesses is similar. This also helped to rule out the increased thickness of the meso-C devices as contributing to the slow transient response. The performance of these standard architecture devices is somewhat lower than literature reports of similar devices (see the Supporting Information). This is predominantly due to the increased thickness of the mesoporous layers; high performance devices in literature often use very thin mesoporous TiO_2 layers of 100−200 nm. Nevertheless, they still allow us to make clear comparisons between the different architectures used in this study.

An interesting factor of the AVA cation is the presence of the carboxylic acid group, which may adsorb to the metal oxide nanoparticle surface. Therefore, it cannot be assumed that it can be treated the same as other larger cation molecules that have been shown to form 2D lead iodide perovskites. The fact that XRD patterns only reveal the low-dimensional perovskite present in higher concentrations of AVA:MAPI perovskites could be that the AVA preferentially adsorbs to the metal oxide rather than being available to form the interlayers between 3D perovskite regions.[21]

FT-IR measurements (see the Supporting Information) were used to confirm the adsorption of AVA on both TiO_2 and ZrO_2 mesoporous layers. The presence of the AVA molecule on the surface of the metal oxides is evidenced by the C−H stretching band at around 2990 cm^{-1} for both the pure powder and the AVA immersed TiO_2 and ZrO_2 samples. For the pure AVA powder, the C═O stretching band was observed at 1709 cm^{-1}. This band was not present for the samples of TiO_2 or ZrO_2 that had been immersed in AVA solution, showing that the molecule anchored to the metal oxide via the carboxylic acid group.[40]

Hu et al. have shown that AVA helps to speed up charge extraction at the TiO_2 interface.[13] They observe a decrease in the lifetime of the time-resolved photoluminescence signal, associated with improved quenching, for AVA containing perovskite compared to pure MAPI. Transient photovoltage measurements do not resolve transport or charge extraction processes, only the impact that changes in these have on recombination; potentially slower charge extraction may lead to accumulation of charges and increased recombination. We do not see an obvious difference on the recombination kinetics in mesoporous TiO_2 spiro-OMeTAD based devices with or without the AVA additive. The V_{oc} rise is comparable for both devices (Figure 6a). While the negative transient is present in both cases it decays at the same relatively fast rate (within 20 s) as shown in Figure 6b. This shows that any change in the rate of charge extraction from the perovskite layer does not result in significant charge accumulation and increased surface recombination.

The very slow dynamics can also not be reproduced in devices with only a mesoporous ZrO_2 layer—note that these devices still contain a compact TiO_2 blocking layer as the electron extracting contact. The magnitude of the negative transient was larger for the device containing the AVA additive in the perovskite, but the rate at which it decreased was comparable to that of the pure MAPI device (Figure 7). The

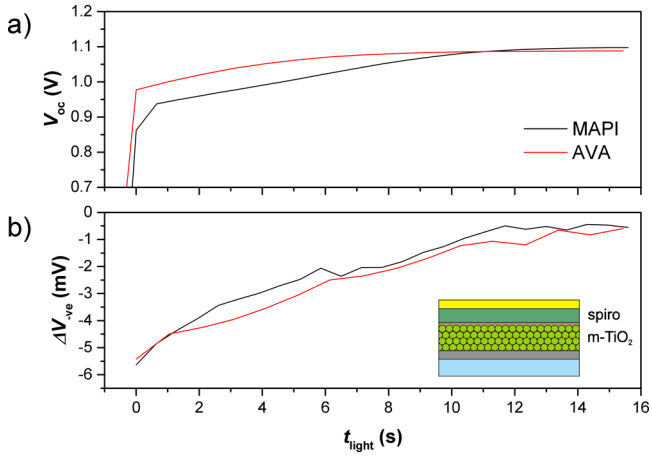

Figure 6. V_{oc} rise (a) and amplitude of the negative transient for mesoporous TiO_2/spiro cells containing pure MAPI and AVA additive perovskite (b).

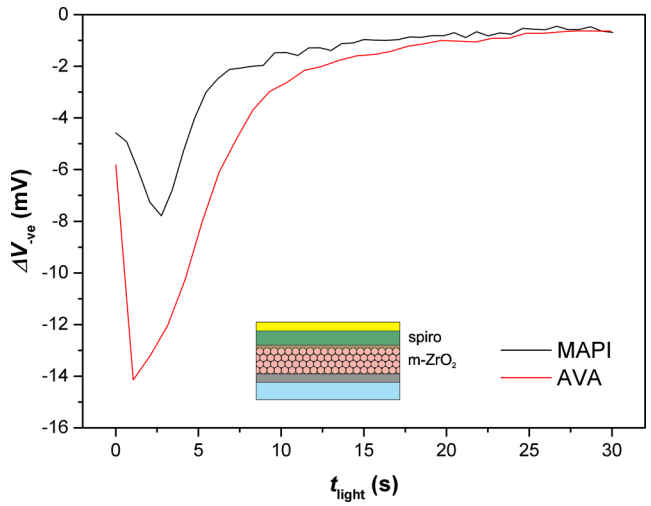

Figure 7. Amplitude of the negative transient for ZrO_2/spiro cells containing pure MAPI and AVA additive perovskite.

apparent increased recombination in the AVA device is consistent with the lower *JV* performance compared to the MAPI cells (see the Supporting Information) and is likely to be the result of a nonoptimized perovskite deposition in the case of the ZrO_2 architecture. None of the devices were fully optimized, as the main comparison of interest was the effect the different perovskite solutions had on the same architecture; i.e., it is difficult to draw comparisons between the behavior of TiO_2 cells and TiO_2 + ZrO_2 cells as their relative performances were different. The key observation is whether or not there is a significant difference in the rate of the negative transient behavior for the AVA additive perovskite compared to that of pure MAPI in each architecture.

The presence of the AVA additive in cells containing both mesoporous TiO_2 + ZrO_2 can be seen to have an impact on the rate of the negative transient decay as shown in Figure 8. The rate at which the negative spike disappears is around 10 times slower for cells with the AVA additive versus the pure MAPI perovskite. In the case of the pure MAPI, the exponential curve in Figure 8 shows a single time constant of approximately 1.15 s. For the AVA device, the negative transient decay curve shows two time constants: a faster

DOI: 10.1021/acs.jpcc.9b01058
J. Phys. Chem. C 2019, 123, 11414−11421

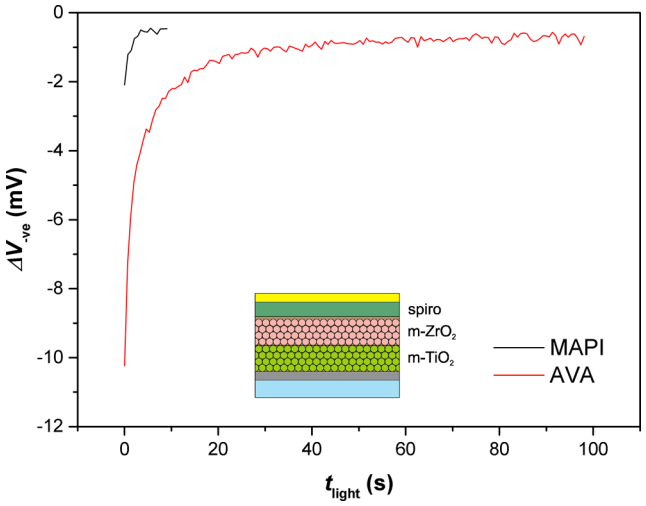

Figure 8. Amplitude of the negative transient for TiO_2/ZrO_2/spiro cells containing pure MAPI and AVA additive perovskite.

process similar to that for the pure MAPI cell (t_1 = 1.09 s) and an additional slower process with a time constant of 11.0 s. This result is consistent with the exceptionally slow response times observed in the meso-C cells containing the AVA additive. Here we have recreated the comparable effect (order of magnitude increase) in devices with a mesoporous TiO_2 and ZrO_2 layer, which suggests that the combination of the interface between the two metal oxides and the presence of AVA is responsible for this behavior.

Studying the meso-C devices TPV behavior with different laser wavelengths, essentially changing light penetration depth, also infers that this TiO_2/ZrO_2 interface may be the location of the increased surface recombination. The negative transient response is more prominent when the cell is probed with a longer wavelength red laser compared to using blue (see the Supporting Information). The longer wavelength light will penetrate deeper into the device, approaching the ZrO_2 layer, whereas the blue laser light will likely be absorbed in the first few tens of nanometers.

Examples of the importance of the TiO_2/ZrO_2 interface in the presence of AVA have also been shown in the literature when studying the infiltration of the perovskite solution through the device. Mei et al. observed that infiltration from the ZrO_2 into the TiO_2 was substantially improved in the presence of AVA.[22] This suggests that the AVA may be adsorbed at this interface, allowing better wetting of the underlying TiO_2 mesoporous layer through changes in surface energy. This effect has more recently been studied in detail using a range of techniques by our co-workers.[41]

CONCLUSIONS

We have demonstrated the exceptionally slow response time under illumination of mesoporous carbon based perovskite cells containing AVA as an additive. TPV measurements during the slow rise in V_{oc} in response to illumination show a clear link between surface recombination and ionic movement. Temperature-dependent measurements revealed that the process was still associated with iodide ion migration via vacancies as shown by the comparable activation energy as found in other studies. However, the typical rate of V_{oc} rise in these cells is at least 1 order of magnitude slower than for standard spiro-OMeTAD devices with several minutes of illumination being required in order to reach a steady state. We attribute this slow rate to the presence of the AVA additive—it is possible that the AVA forms 2D perovskite regions which restrict ion migration. We have also confirmed that the AVA can adsorb on the TiO_2 and ZrO_2 surfaces via its carboxylic acid group. This anchored charged molecule could also inhibit ion migration via electrostatic interaction. It is likely that reduced iodide ion movement is linked to the improved stability observed in devices with the AVA additive.

To attempt to uncover the location of the dominant recombination process impacting the slow electronic response, we simplified the device structure to a more conventional approach with spiro-OMeTAD as the HTL. By varying the mesoporous metal oxide layers in the device we revealed that the AVA additive only induces the slow response when both mesoporous TiO_2 and ZrO_2 are present. This suggests that the AVA acts at the interface between these two layers to slow ionic movement. It is not clear whether or not the AVA preferentially binds to the ZrO_2 as the perovskite solution is infiltrated from the top of the device, or perhaps builds up at the interface due to the misalignment between pores in the two layers. Optimization of this interface would provide important benefits when deploying these cells in the real world, since such a slow response time would give inferior performance under changeable light conditions.

ASSOCIATED CONTENT

Supporting Information

The Supporting Information is available free of charge on the ACS Publications website at DOI: 10.1021/acs.jpcc.9b01058.

JV device performance, FTIR of AVA on TiO_2 and ZrO_2, TPV transient progression of standard cells, and TPV measurements with different wavelength lasers (PDF)

AUTHOR INFORMATION

Corresponding Authors

*(A.P.) E-mail: adam.pockett@swansea.ac.uk. Telephone: +44 1792 60 6646.

*(M.C.) E-mail: m.j.carnie@swansea.ac.uk. Telephone: +44 1792 60 6489.

ORCID

Adam Pockett: 0000-0002-4747-9560

Matthew Carnie: 0000-0002-4232-1967

Author Contributions

The manuscript was written through contributions of all authors.

Notes

The authors declare no competing financial interest.

All data created during this research are openly available from the Swansea University data archive at http://doi.org/10.5281/zenodo.2555145.

ACKNOWLEDGMENTS

The authors would like to thank the EPSRC (EP/N020863/1, EP/R032750/1, EP/M015254/2, EP/P032591/1), the Welsh European Funding Office (SPARC II), and the Welsh Government's Sêr Solar programme for funding.

DOI: 10.1021/acs.jpcc.9b01058
J. Phys. Chem. C 2019, 123, 11414−11421

REFERENCES

(1) Cotella, G.; Baker, J.; Worsley, D.; De Rossi, F.; Pleydell-Pearce, C.; Carnie, M.; Watson, T. One-step Deposition by Slot-die Coating of Mixed Lead Halide Perovskite for Photovoltaic Applications. *Sol. Energy Mater. Sol. Cells* **2017**, *159*, 362−369.

(2) Hwang, K.; Jung, Y.-S.; Heo, Y.-J.; Scholes, F. H.; Watkins, S. E.; Subbiah, J.; Jones, D. J.; Kim, D.-Y.; Vak, D. Toward Large Scale Roll-to-Roll Production of Fully Printed Perovskite Solar Cells. *Adv. Mater.* **2015**, *27*, 1241−1247.

(3) Burkitt, D.; Searle, J.; Watson, T. Perovskite Solar Cells in N-I-P Structure With Four Slot-die-coated Layers. *R. Soc. Open Sci.* **2018**, *5*, 172158.

(4) Wei, Z.; Chen, H.; Yan, K.; Yang, S. Inkjet Printing and Instant Chemical Transformation of a $CH_3NH_3PbI_3$/Nanocarbon Electrode and Interface for Planar Perovskite Solar Cells. *Angew. Chem., Int. Ed.* **2014**, *53*, 13239−13243.

(5) Li, S.-G.; Jiang, K.-J.; Su, M.-J.; Cui, X.-P.; Huang, J.-H.; Zhang, Q.-Q.; Zhou, X.-Q.; Yang, L.-M.; Song, Y.-L. Inkjet Printing of $CH_3NH_3PbI_3$ on a Mesoscopic TiO_2 Film for Highly Efficient Perovskite Solar Cells. *J. Mater. Chem. A* **2015**, *3*, 9092−9097.

(6) Liu, M.; Johnston, M. B.; Snaith, H. J. Efficient Planar Heterojunction Perovskite Solar Cells by Vapour Deposition. *Nature* **2013**, *501*, 395.

(7) Borchert, J.; Milot, R. L.; Patel, J. B.; Davies, C. L.; Wright, A. D.; Martínez Maestro, L.; Snaith, H. J.; Herz, L. M.; Johnston, M. B. Large-Area, Highly Uniform Evaporated Formamidinium Lead Triiodide Thin Films for Solar Cells. *ACS Energy Lett.* **2017**, *2*, 2799−2804.

(8) Cao, K.; Zuo, Z.; Cui, J.; Shen, Y.; Moehl, T.; Zakeeruddin, S. M.; Grätzel, M.; Wang, M. Efficient Screen Printed Perovskite Solar Cells Based on Mesoscopic TiO_2/Al_2O_3/NiO/Carbon Architecture. *Nano Energy* **2015**, *17*, 171−179.

(9) Ku, Z.; Rong, Y.; Xu, M.; Liu, T.; Han, H. Full Printable Processed Mesoscopic $CH_3NH_3PbI_3$/TiO_2 Heterojunction Solar Cells With Carbon Counter Electrode. *Sci. Rep.* **2013**, *3*, 3132−3132.

(10) Baker, J.; Hooper, K.; Meroni, S.; Pockett, A.; McGettrick, J.; Wei, Z.; Escalante, R.; Oskam, G.; Carnie, M.; Watson, T. High Throughput Fabrication of Mesoporous Carbon Perovskite Solar Cells. *J. Mater. Chem. A* **2017**, *5*, 18643−18650.

(11) Meroni, S. M. P.; Mouhamad, Y.; De Rossi, F.; Pockett, A.; Baker, J.; Escalante, R.; Searle, J.; Carnie, M. J.; Jewell, E.; Oskam, G.; et al. Homogeneous and Highly Controlled Deposition of Low Viscosity Inks and Application on Fully Printable Perovskite Solar Cells. *Sci. Technol. Adv. Mater.* **2018**, *19*, 1−9.

(12) De Rossi, F.; Baker, J. A.; Beynon, D.; Hooper, K. E. A.; Meroni, S. M. P.; Williams, D.; Wei, Z.; Yasin, A.; Charbonneau, C.; Jewell, E. H.; et al. All Printable Perovskite Solar Modules with 198 cm^2 Active Area and Over 6% Efficiency. *Adv. Mater. Technol.* **2018**, *3*, 1800156.

(13) Hu, Y.; Zhang, Z.; Mei, A.; Jiang, Y.; Hou, X.; Wang, Q.; Du, K.; Rong, Y.; Zhou, Y.; Xu, G.; et al. Improved Performance of Printable Perovskite Solar Cells with Bifunctional Conjugated Organic Molecule. *Adv. Mater.* **2018**, *30*, 1705786.

(14) Zhang, Y.-Y.; et al. Intrinsic Instability of the Hybrid Halide Perovskite Semiconductor $CH_3NH_3PbI_3$. *Chin. Phys. Lett.* **2018**, *35*, 036104.

(15) Bryant, D.; Aristidou, N.; Pont, S.; Sanchez-Molina, I.; Chotchunangatchaval, T.; Wheeler, S.; Durrant, J. R.; Haque, S. A. Light and Oxygen Induced Degradation Limits the Operational Stability of Methylammonium Lead Triiodide Perovskite Solar Cells. *Energy Environ. Sci.* **2016**, *9*, 1655−1660.

(16) Niu, G.; Li, W.; Meng, F.; Wang, L.; Dong, H.; Qiu, Y. Study on the Stability of $CH_3NH_3PbI_3$ Films and the Effect of Post-modification by Aluminum Oxide in All-solid-state Hybrid Solar Cells. *J. Mater. Chem. A* **2014**, *2*, 705−710.

(17) Saliba, M.; Matsui, T.; Seo, J.-Y.; Domanski, K.; Correa-Baena, J.-P.; Nazeeruddin, M. K.; Zakeeruddin, S. M.; Tress, W.; Abate, A.; Hagfeldt, A.; et al. Cesium-containing Triple Cation Perovskite Solar Cells: Improved Stability, Reproducibility and High Efficiency. *Energy Environ. Sci.* **2016**, *9*, 1989−1997.

(18) Tsai, H.; Nie, W.; Blancon, J.-C.; Stoumpos, C. C.; Asadpour, R.; Harutyunyan, B.; Neukirch, A. J.; Verduzco, R.; Crochet, J. J.; Tretiak, S.; et al. High-efficiency Two-dimensional Ruddlesden−Popper Perovskite Solar Cells. *Nature* **2016**, *536*, 312.

(19) Milot, R. L.; Sutton, R. J.; Eperon, G. E.; Haghighirad, A. A.; Martinez Hardigree, J.; Miranda, L.; Snaith, H. J.; Johnston, M. B.; Herz, L. M. Charge-Carrier Dynamics in 2D Hybrid Metal−Halide Perovskites. *Nano Lett.* **2016**, *16*, 7001−7007.

(20) Smith, I. C.; Hoke, E. T.; Solis-Ibarra, D.; McGehee, M. D.; Karunadasa, H. I. A Layered Hybrid Perovskite Solar-Cell Absorber with Enhanced Moisture Stability. *Angew. Chem., Int. Ed.* **2014**, *53*, 11232−11235.

(21) Grancini, G.; Roldán-Carmona, C.; Zimmermann, I.; Mosconi, E.; Lee, X.; Martineau, D.; Narbey, S.; Oswald, F.; De Angelis, F.; Graetzel, M.; et al. One-Year Stable Perovskite Solar Cells by 2D/3D Interface Engineering. *Nat. Commun.* **2017**, *8*, 15684.

(22) Mei, A.; Li, X.; Liu, L.; Ku, Z.; Liu, T.; Rong, Y.; Xu, M.; Hu, M.; Chen, J.; Yang, Y.; et al. A Hole-conductor−free, Fully Printable Mesoscopic Perovskite Solar Cell With High Stability. *Science* **2014**, *345*, 295−298.

(23) Bliss, M.; Smith, A.; Betts, T. R.; Baker, J.; De Rossi, F.; Bai, S.; Watson, T.; Snaith, H.; Gottschalg, R. Spectral Response Measurements of Perovskite Solar Cells. *IEEE J. Photovolt.* **2019**, *9*, 220−226.

(24) Eames, C.; Frost, J. M.; Barnes, P. R. F.; O'Regan, B. C.; Walsh, A.; Islam, M. S. Ionic Transport in Hybrid Lead Iodide Perovskite Solar Cells. *Nat. Commun.* **2015**, *6*, 7497.

(25) Pockett, A.; Eperon, G. E.; Sakai, N.; Snaith, H. J.; Peter, L. M.; Cameron, P. J. Microseconds, Milliseconds and Seconds: Deconvoluting the Dynamic Behaviour of Planar Perovskite Solar Cells. *Phys. Chem. Chem. Phys.* **2017**, *19*, 5959−5970.

(26) Azpiroz, J. M.; Mosconi, E.; Bisquert, J.; De Angelis, F. Defect Migration in Methylammonium Lead Iodide and Its Role in Perovskite Solar Cell Operation. *Energy Environ. Sci.* **2015**, *8*, 2118−2127.

(27) Snaith, H. J.; Abate, A.; Ball, J. M.; Eperon, G. E.; Leijtens, T.; Noel, N. K.; Stranks, S. D.; Wang, J. T.-W.; Wojciechowski, K.; Zhang, W. Anomalous Hysteresis in Perovskite Solar Cells. *J. Phys. Chem. Lett.* **2014**, *5*, 1511−1515.

(28) Calado, P.; Burkitt, D.; Yao, J.; Troughton, J.; Watson, T. M.; Carnie, M. J.; Telford, A. M.; O'Regan, B. C.; Nelson, J.; Barnes, P. R. F. Identifying Dominant Recombination Mechanisms in Perovskite Solar Cells by Measuring the Transient Ideality Factor. *Phys. Rev. Appl.* **2019**, *11*, 044005.

(29) Pockett, A.; Carnie, M. J. Ionic Influences on Recombination in Perovskite Solar Cells. *ACS Energy Lett.* **2017**, *2*, 1683−1689.

(30) Calado, P.; Telford, A. M.; Bryant, D.; Li, X.; Nelson, J.; O'Regan, B. C.; Barnes, P. R. F. Evidence for Ion Migration in Hybrid Perovskite Solar Cells With Minimal Hysteresis. *Nat. Commun.* **2016**, *7*, 13831.

(31) Baumann, A.; Väth, S.; Rieder, P.; Heiber, M. C.; Tvingstedt, K.; Dyakonov, V. Identification of Trap States in Perovskite Solar Cells. *J. Phys. Chem. Lett.* **2015**, *6*, 2350−2354.

(32) Xing, J.; Wang, Q.; Dong, Q.; Yuan, Y.; Fang, Y.; Huang, J. Ultrafast Ion Migration in Hybrid Perovskite Polycrystalline Thin Films Under Light and Suppression in Single Crystals. *Phys. Chem. Chem. Phys.* **2016**, *18*, 30484−30490.

(33) Haruyama, J.; Sodeyama, K.; Han, L.; Tateyama, Y. First-Principles Study of Ion Diffusion in Perovskite Solar Cell Sensitizers. *J. Am. Chem. Soc.* **2015**, *137*, 10048−10051.

(34) Delugas, P.; Caddeo, C.; Filippetti, A.; Mattoni, A. Thermally Activated Point Defect Diffusion in Methylammonium Lead Trihalide: Anisotropic and Ultrahigh Mobility of Iodine. *J. Phys. Chem. Lett.* **2016**, *7*, 2356−2361.

(35) Hoque, M. N. F.; Islam, N.; Li, Z.; Ren, G.; Zhu, K.; Fan, Z. Ionic and Optical Properties of Methylammonium Lead Iodide Perovskite across the Tetragonal−Cubic Structural Phase Transition. *ChemSusChem* **2016**, *9*, 2692−2698.

DOI: 10.1021/acs.jpcc.9b01058
J. Phys. Chem. C 2019, 123, 11414−11421

(36) Yu, H.; Lu, H.; Xie, F.; Zhou, S.; Zhao, N. Native Defect-Induced Hysteresis Behavior in Organolead Iodide Perovskite Solar Cells. *Adv. Funct. Mater.* **2016**, *26*, 1411−1419.
(37) Yang, D.; Ming, W.; Shi, H.; Zhang, L.; Du, M.-H. Fast Diffusion of Native Defects and Impurities in Perovskite Solar Cell Material $CH_3NH_3PbI_3$. *Chem. Mater.* **2016**, *28*, 4349−4357.
(38) Meggiolaro, D.; Mosconi, E.; De Angelis, F. Modeling the Interaction of Molecular Iodine with $MAPbI_3$: A Probe of Lead-Halide Perovskites Defect Chemistry. *ACS Energy Lett.* **2018**, *3*, 447−451.
(39) Aristidou, N.; Eames, C.; Sanchez-Molina, I.; Bu, X.; Kosco, J.; Islam, M. S.; Haque, S. A. Fast Oxygen Diffusion and Iodide Defects Mediate Oxygen-induced Degradation of Perovskite Solar Cells. *Nat. Commun.* **2017**, *8*, 15218.
(40) Ooyama, Y.; Furue, K.; Enoki, T.; Kanda, M.; Adachi, Y.; Ohshita, J. Development of Type-I/Type-II Hybrid Dye Sensitizer With Both Pyridyl Group and Catechol Unit as Anchoring Group for Type-I/Type-II Dye-sensitized Solar Cell. *Phys. Chem. Chem. Phys.* **2016**, *18*, 30662−30676.
(41) Lakhiani, H.; Dunlop, T.; De Rossi, F. D.; Dimitrov, S.; Kerremans, R.; Charbonneau, C.; Watson, T.; Barbé, J.; Tsoi, W. C. Variations of Infiltration and Electronic Contact in Mesoscopic Perovskite Solar Cells Revealed by High-resolution Multi-mapping Techniques. *Adv. Funct. Mater.* **2019**, 1900885.

DOI: 10.1021/acs.jpcc.9b01058
J. Phys. Chem. C 2019, 123, 11414−11421